23PM3F-02

Hidden Rays on the Shadow Boundaries of Penetrable Wedges

Se-Yun Kim [#]

[#] *Imaging Media Research Center, Korea Institute of Science and Technology*
5 Gil 14 Hwarangro, Sungbuk-gu, Seoul, 136-791, Korea
ksy@imrc.kist.re.kr

***Abstract*—Reflection and refraction of ordinary rays occur only on lit boundary without considering the field singularity at edges. In electromagnetic diffraction by a wedge, a systematic way on tracing hidden rays reflected and refracted on its shadow boundary was implemented in the complementary regions, which were well defined in the formulation of dual integral equations. And then, the angular period of its extended physical optics (PO) diffraction coefficients are adjusted to satisfy the edge condition at wedge tip. This procedure is applied to E-polarized diffraction by a composite wedge composed of a perfect conductor and a lossy dielectric. The diffraction coefficients and field patterns are plotted here, and compared to the conventional PO solution.**

I. INTRODUCTION

The geometrical theory of diffraction (GTD) [1] was developed by extracting a generalization of Fermat's principle on diffracted rays from the second term of the exact asymptotic series solution to a perfectly conducting wedge. But the application of the GTD and its improved versions to penetrable scatterers has been hampered by the lack of exact diffraction coefficients of penetrable wedges [2]. The above limitation led many researchers to calculate the diffraction coefficients of a penetrable wedge heuristically [3] and numerically [4]. In spite of highly accurate results, the heuristic and numerical techniques could not provide comparable achievements in the physical understanding of penetrable wedge diffractions. A simplest way to obtain an approximate but analytic expression on the diffraction coefficients of penetrable wedges may be the physical optics (PO) approximation [5]. In view of the physical theory of diffraction (PTD) [6], the error of PO solutions may be generated by the lack of nonuniform currents.

In general, a PO solution denotes the field radiated from uniform currents, which are obtained only by conventional geometrical optics (GO) fields on lit boundaries. And GO fields can be expressed only by ordinary ray-tracing data in the physical regions. Recently, a systematic way on tracing hidden rays reflected and refracted on its shadow boundary was implemented in the complementary regions, which were well defined in the formulation of dual integral equations. And then, the angular period of its extended physical optics (PO) diffraction coefficients are adjusted to satisfy the edge condition at wedge tip. The hidden rays of diffraction (HRD) [7],[8] procedure is applied to E-polarized diffraction by a composite wedge composed of a perfect conductor and a lossy dielectric. The diffraction coefficients and field patterns are plotted here, and compared to the conventional PO solution. The $\exp(-i\omega t)$ time convention is adopted and suppressed here.

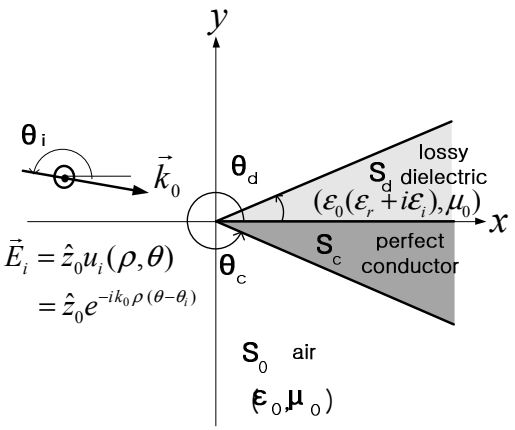

Fig. 1. E-polarized diffraction by a composite wedge composed of a perfect conductor and a lossy dielectric

II. FORMULATION OF DUAL INTEGRAL EQUATIONS

Fig. 1 shows the geometry of a composite wedge composed of a perfect conductor in S_c and a lossy dielectric with complex relative dielectric constant $\varepsilon^*(=\varepsilon_r+i\varepsilon_i)$ in S_d. The air region S_0 consists of two boundaries at $\theta=\theta_d$ and θ_c, which satisfy $\pi<\theta_c-\theta_d<2\pi$. When an E-polarized unit plane wave $u_i(\rho,\theta)$ is incident on the composite wedge, the z-component of the total electric field $u(\rho,\theta)$ is formulated into the dual integral equations [5]

$$u_i(\rho,\theta)-F^{-1}\left[\frac{J_c(\alpha,\beta)+J_d(\alpha,\beta)+M_d(\alpha,\beta)}{\alpha^2+\beta^2-k_0^2}\right] = \begin{cases} u(\rho,\theta), & in \quad S_0 \quad (1a) \\ 0, & in \quad S_c^{(0)}+S_d^{(0)} \quad (1b) \end{cases}$$

$$F^{-1}\left[\frac{J_d(\alpha,\beta)+M_d(\alpha,\beta)+J_0(\alpha,\beta)}{\alpha^2+\beta^2-k_d^2}\right] = \begin{cases} u(\rho,\theta), & in \quad S_d \quad (2a) \\ 0, & in \quad S_c^{(d)}+S_0^{(d)} \quad (2b) \end{cases}$$

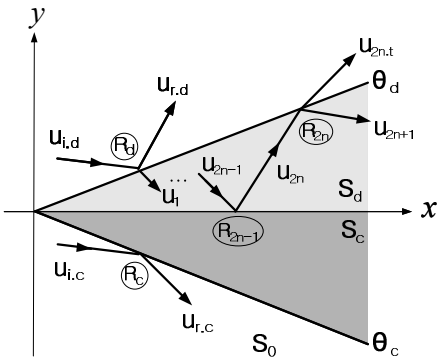

Fig. 2. Ordinary ray-tracing in case that both boundaries are illuminated by an E-polarized plane wave

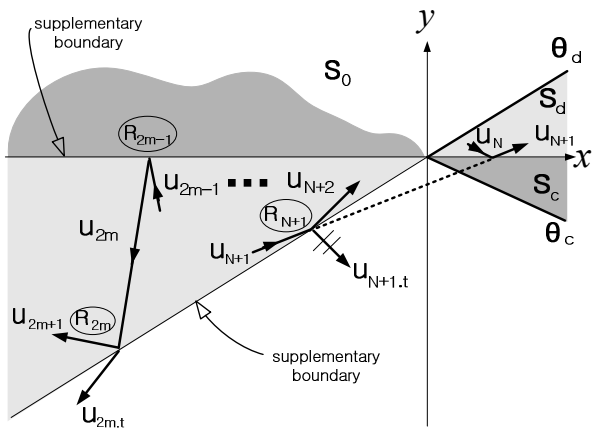

Fig. 3. Hidden ray-tracing in case that the last ordinary reflection occurs on the conducting boundary inside the lossy dielectric

where $k_0 = w\sqrt{\varepsilon_0\mu_0}$ and $k_d = k_0\sqrt{\varepsilon^*}$ denote the wavenumbers in S_0 and S_d, respectively. And the operator F^{-1} denotes two-dimensional inverse Fourier transform. Four spectral functions of J_c, J_d, M_d, and J_0 are well defined in [7].

In (1b), $S_c^{(0)}$ and $S_d^{(0)}$ denote the complementary regions of S_c and S_d, respectively, of which media are replaced by air. Then (1) implies that both the induced currents J_c at $\theta = \theta_c$ and $J_d + M_d$ at $\theta = \theta_d$ not only generate the scattered field in S_0, but also cancel out the incident field in $S_c^{(0)}$ and $S_d^{(0)}$. In the same manner, $S_c^{(d)}$ and $S_0^{(d)}$ in (2b) denote the complementary dielectric regions corresponding to S_c and S_0, respectively. Then (2) describes such a radiation phenomenon that both the induced currents J_0 at $\theta = 0$ and $J_d + M_d$ at $\theta = \theta_d$ provide not only the total field in S_d but also null-field in $S_c^{(d)}$ and $S_0^{(d)}$. If four spectral functions of J_c, J_d, M_d, and J_0 are known exactly, the exact field $u(\rho,\theta)$ can be obtained from (1a) and (2a). Unfortunately, there is no mathematical way to obtain those spectral functions exactly. However, both (1b) and (2b) should be absolutely satisfied if $u(\rho,\theta)$ becomes exact. Hence (1b) and (2b), called the null-field condition in the complementary regions, play a vital role in verifying the accuracy of an approximately constructed solution of $u(\rho,\theta)$.

III. Ordinary and Hidden Ray-Tracings

To obtain an approximate but analytic expression on the diffraction coefficients of a penetrable wedge, the simplest way may be the conventional physical optics (PO) approximation [5]. The PO solution can be easily constructed by replacing the exact fields on the wedge boundaries by the conventional GO field $u_g(\rho,\theta)$. As shown in Fig. 2, ordinary ray-tracing provides the conventional GO field. It should be noted that the modified propagation constants [9] are employed here to provide the GO field including the multiple reflections inside the lossy dielectric.

Fig. 3 illustrates the generation of the first hidden ray u_{N+1} inside the complementary dielectric region after the last ordinary ray u_{N+1} is captured inside the physical dielectric region. And the first hidden ray u_{N+1} is incident on the supplementary dielectric boundary. Then, one may easily trace the reflected ray u_{N+2}. Let u_{2m-1} denote the hidden ray undergoing the $(2m-2-N)$-th reflection from the first hidden ray u_{N+1}. The hidden ray u_{2m} is incident on the supplementary dielectric boundary, and then generates the reflected ray u_{2m+1} and the refracted ray $u_{2m.t}$. The real and imaginary angles of $u_{2m.t}$ and u_{2m+1} are easily determined by the Snell's law. The amplitudes of the ordinary and hidden rays are easily calculated by multiplication of the Fresnel's reflection coefficients.

IV. Construction of Diffraction Coefficients

The procedure on the construction of the diffraction coefficients from the ray-tracing data is illustrated in Fig. 4. The diffraction coefficients are expressed by the same number of cotangent functions as sum of the total numbers of the ordinary and hidden rays. The pole and amplitude of a cotangent function are taken by the propagation angle and amplitude of the corresponding ordinary or hidden ray, respectively. And then, the angular period of the cotangent functions is changed into $2\pi\nu_r$. The constant ν_r is taken by the minimum positive real value satisfying the edge condition [10] near the composite wedge tip as

$$(\varepsilon_r + i\varepsilon_i)\tan\left(\frac{\theta_d - \theta_c}{\nu_r + i\nu_i}\right) = \tan\left(\frac{\theta_d}{\nu_r + i\nu_i}\right) \tag{3}$$

Hence, the multiple reflection inside the lossy dielectric in Fig. 3 should continue until any hidden ray cannot penetrate into the next physical regions $[2\pi\nu_r, \theta_d + 2\pi\nu_r]$ or $[-2\pi\nu_r, \theta_d - 2\pi\nu_r]$.

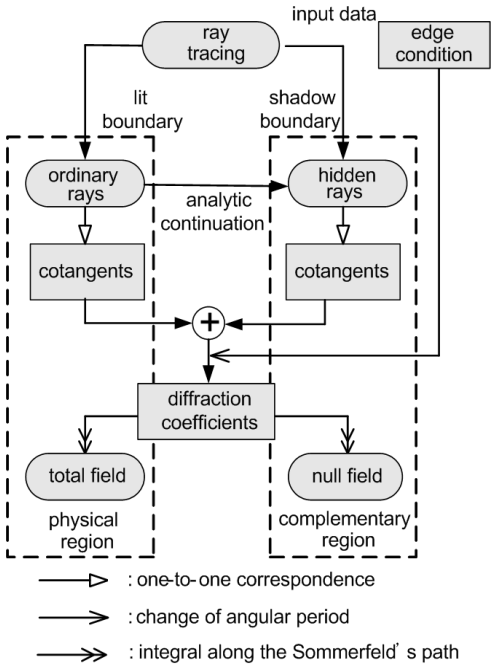

Fig. 4. The procedure on constructing the diffraction coefficients from the ordinary and hidden ray-tracing data and edge condition

Then, the total fields in the physical and complementary air regions are expressed by the sum of the conventional GO field $u_g(\rho,\theta)$ and the edge-diffracted field, which is given by the asymptotic integral form as

$$u(\rho,\theta)=u_g(\rho,\theta)+\frac{1}{2\pi i}\int_{SDP}\begin{Bmatrix} f_{1c}^{(c)}(w)+f_{1d}^{(c)}(w+2\pi) \\ f_{1c}^{(c)}(w)+f_{1d}^{(c)}(w) \\ f_{1c}^{(c)}(w-2\pi)+f_{1d}^{(c)}(w)\end{Bmatrix} \times e^{ik_0\rho\cos(w-\theta)}dw, \quad in \begin{cases} 0\le\theta<\theta_d & (4a)\\ \theta_d\le\theta\le\theta_c & (4b)\\ \theta_c<\theta\le 2\pi & (4c)\end{cases}$$

where SDP denotes the steepest decent path in asymptotic integral [11]. And two diffraction coefficients in (4), $f_{1c}^{(c)}(w)$ and $f_{1d}^{(c)}(w)$ are given by

$$f_{1c}^{(c)}(w)=-\frac{1}{2\nu_r}\left[\cot\left(\frac{w-\theta_{i.c}}{2\nu_r}\right)+R_c\cot\left(\frac{w-\theta_{r.c}}{2\nu_r}\right)\right] \quad (5a)$$

$$f_{1d}^{(c)}(w)=\frac{1}{2\nu_r}\left[\cot\left(\frac{w-\theta_{i.d}}{2\nu_r}\right)+R_d\cot\left(\frac{w-\theta_{r.d}}{2\nu_r}\right)+\sum_{m=1}^{M}K_{2m.t}\cot\left(\frac{w-\theta_{2m.t}^{*}}{2\nu_r}\right)\right]. \quad (5b)$$

All of the value required in (5) can be easily obtained only from the ray-tracing data and the edge condition.

In (4), the diffraction coefficients $f_{1c}^{(c)}(w)$ and $f_{1d}^{(c)}(w)$ are

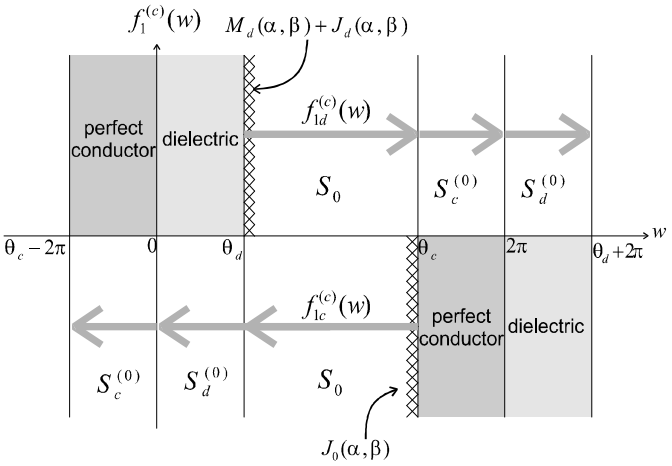

Fig. 5. Radiation of the induced currents into the physical and complementary air regions

generated from the induced currents $J_d(\alpha,\beta)+M_d(\alpha,\beta)$ at $\theta=\theta_d$ and $J_c(\alpha,\beta)$ at $\theta=\theta_c$, respectively. As shown in Fig. 5, $f_{1d}^{(c)}(w)$ and $f_{1c}^{(c)}(w)$ exist in the same physical air region S_0 ($\theta_d\le\theta\le\theta_c$) simultaneously. But $f_{1d}^{(c)}(w)$ and $f_{1c}^{(c)}(w)$ are not overlapped in the same complementary air regions due to those opposite radiation directions. It leads us to express (4) in case that $S_d^{(0)}$ and $S_c^{(0)}$ are fixed in the regions $0\le\theta<\theta_d$ and $\theta_c<\theta\le 2\pi$, respectively.

V. Results and Discussions

Both PO and HRD diffraction coefficients in the physical and complementary air regions are plotted for $\theta_d=60^\circ$, $\theta_c=330^\circ$, $\theta_i=170^\circ$, and $\varepsilon_r=1.01$. In Fig. 6, the broken and dotted lines marked by $\varepsilon_i=0$ and ∞ denote the exact diffraction coefficients of the perfectly conducting wedges with $\theta_d=0^\circ$ and 60°, respectively. Figs. 6(a) and (b) show the PO and HRD diffraction coefficients as ε_i increases from 0.1 to 100, respectively. Unlike the PO diffraction coefficients, the HRD curves in Fig. 6(b) approach to the corresponding exact diffraction coefficients as ε_i increases to 100 or decreases to 0.1. The HRD curves provide smooth transition from low to high ε_i. The accuracy of the HRD diffraction coefficients is assured by showing how closely the null field condition is satisfied in the complementary air regions.

Figs. 7(a) and (b) show the edge-diffracted and total fields calculated at 1.5 wavelength away from the wedge tip for $\theta_d=60^\circ$, $\theta_c=330^\circ$, $\theta_i=170^\circ$, $\varepsilon_r=1.01$, and $\varepsilon_i=0.01$. The broken line denotes the exact field of the perfectly conducting wedges with $\theta_d=0^\circ$. As expected, the PO fields (blue lines) suffer from large deviation from the exact pattern. In contrast, the HRD fields (red lines) approach to the exact pattern very closely.

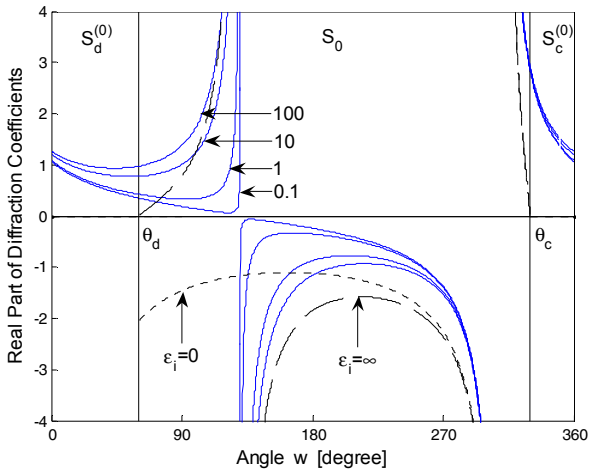

(a) PO

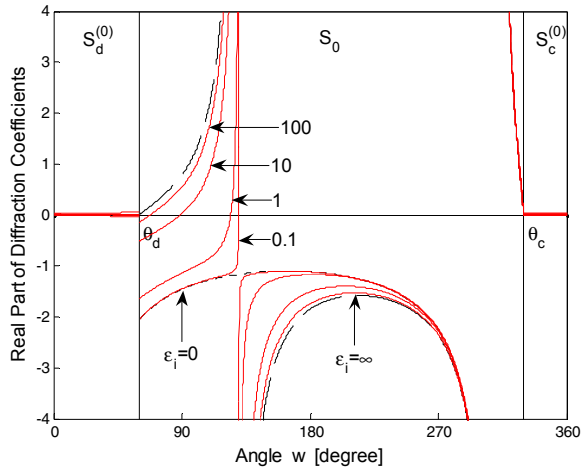

(b) HRD

Fig. 6. Real parts of the diffraction coefficients for $\theta_d = 60^\circ$, $\theta_c = 330^\circ$, $\theta_i = 170^\circ$, and $\varepsilon_r = 1.01$ as ε_i increase from 0.1 to 100. The dotted and broken lines denote the exact solutions of the perfectly conducting wedges for $\theta_d = 0°$ and $60°$, respectively.

VI. Conclusion

The lack of induced currents on shadow boundaries and field singularities at edges rendered the conventional PO diffraction coefficients of a wedge to be erroneous. In the HRD technique, hidden ray-tracing on shadow boundaries in complementary regions provides additional diffraction coefficients, of which angular period is also adjusted to satisfy the edge condition at wedge tip. For a composite wedge composed of a perfect conductor and a lossy dielectric, the E-polarized diffraction coefficients and field patterns were plotted in comparison with the conventional PO solution.

Acknowledgment

This work was supported in part by the KIST internal project and in part by the KCC, Korea, under the R&D program supervised by the KCA.

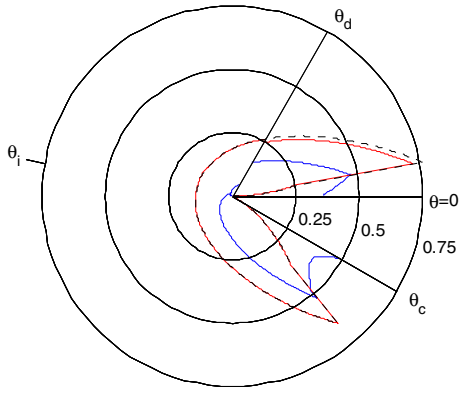

(a) Edge-diffracted fields of PO (blue) and HRD (red)

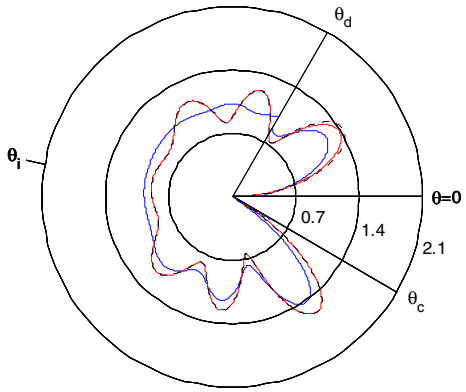

(b) Total fields of PO (blue) and HRD (red)

Fig. 7. Amplitude patterns calculated at 1.5 wavelength away from the wedge tip for $\theta_d = 60^\circ$, $\theta_c = 330^\circ$, $\theta_i = 170^\circ$, $\varepsilon_r = 1.01$, and $\varepsilon_i = 0.01$. The broken line denotes the exact field of the perfectly conducting wedges for $\theta_d = 0°$.

References

[1] J. B. Keller, "Geometrical theory of diffraction," *J. Opt. Soc. Amer.*, vol. 52, pp. 116-130, Feb. 1962.

[2] L. Lewin and L. Sreenivasiah, "Diffraction by a dielectric wedge," Univ. of Colorado, Sci. Rep. 47, 1979.

[3] R. J. Luebbers, "Finite conductivity Uniform GTD versus knife edge diffraction in prediction of propagation path loss," " *IEEE Antennas Propagat.,* vol. 32, pp. 70–76, Jan. 1984.

[4] G. Stritis, V. Anantha, and A. Taflove, "Numerical calculation of diffraction coefficients of generic conducting and dielectric wedges using FDTD," *IEEE Antennas Propagat.,* vol. 45, pp. 1525–1529, Oct. 1997.

[5] S.-Y. Kim, J. W. Ra, and S. Y. Shin, "Diffraction by an arbitrary-angled dielectric wedge," *IEEE Antennas Propagat.,* vol. 39, pp. 1272–1292, Sep. 1991.

[6] P. Ya. Ufimtsev, *Fundamentals of the Physical Theory of Diffraction*, New York: Wiley, 2007.

[7] S.-Y. Kim, "Hidden rays of diffraction," *IEEE Trans. Antennas Propagat.,* vol. 55, pp. 892–906, Mar. 2007.

[8] S.-Y. Kim, "Hidden rays of diffraction for a composite wedge composed of a perfect conductor and a lossy dielectric," *IEICE Trans. Commun.,* vol. E94-B, pp. 484–490, Feb. 2011.

[9] R. D. Radcliff and C. A. Balanis, "Modified propagation constants for nonuniform plane wave transmission through conducting media," *IEEE Geosci. Remote Sens.,* vol. 20, pp. 408–411, Jul. 1982.

[10] J. Meixner, "The behavior of electromagnetic fields at edges," *IEEE Antennas Propagat.,* vol. 20, pp. 442–446, Jul. 1972.

[11] L. B. Felsen and N. Marcuvitz, *Radiation and Scattering of Waves*, Englewood Cliffs, NJ: Prentice-Hall, 1973.